

An X-ray Rietveld and infrared spectral study of the $\text{Na}_2(\text{Mn}_{1-x}\text{M}^{2+})\text{Fe}^{2+}\text{Fe}^{3+}(\text{PO}_4)_3$ ($x = 0$ to 1 and $\text{M}^{2+} = \text{Mg}, \text{Cd}$) alluaudite-type solid solutions

MÉLANIE RONDEUX AND FRÉDÉRIC HATERT*

Laboratoire de Minéralogie, B18, Université de Liège, B-4000 Liège, Belgium

ABSTRACT

Compounds of the $\text{Na}_2(\text{Mn}_{1-x}\text{M}^{2+})\text{Fe}^{2+}\text{Fe}^{3+}(\text{PO}_4)_3$ ($\text{M}^{2+} = \text{Mg}, \text{Cd}, \text{Ca}, \text{Ni}, \text{Zn}$) alluaudite-type solid solutions were synthesized by hydrothermal techniques at 1 kbar, between 400 and 600 °C, and were investigated by X-ray powder diffraction and infrared spectroscopy. The site occupancy factors of the $\text{Na}_2(\text{Mn}_{1-x}\text{Cd}_x)\text{Fe}^{2+}\text{Fe}^{3+}(\text{PO}_4)_3$ compounds, obtained from the Rietveld refinements of the X-ray powder patterns, indicate that the replacement of Mn by Cd mainly takes place on the M1 site. Small amounts of Cd were also detected on the A1 site, compensated by small amounts of Na occurring on M1. The cationic distributions in the $\text{Na}_2(\text{Mn}_{1-x}\text{Mg}_x)\text{Fe}^{2+}\text{Fe}^{3+}(\text{PO}_4)_3$ solid solution show a partially disordered distribution of Fe and Mg over the M1 and M2 crystallographic sites. The unit-cell parameters increase significantly when Mn is replaced by Ca or Cd, and decrease significantly when it is replaced by Ni, Mg, or Zn. The infrared spectra show the displacement of two absorption bands at ca. 405–445 cm^{-1} and 595–610 cm^{-1} , which are assigned to the vibrations of the M^{2+} cations localized on the M1 and M2 sites, respectively. This assignment is confirmed by the excellent correlations between the average ionic radius of the cations occurring on the M sites, and the energy of the absorption band.

Keywords: Crystal chemistry, divalent cation, alluaudite structure, Na-Mn-Fe-phosphate

INTRODUCTION

Phosphates of the alluaudite group occur as accessory minerals in granitic pegmatites, particularly in the beryl-columbite-phosphate subtype of the rare-element pegmatites, according to the classification of Černý and Ercit (2005). The crystal structure of alluaudite from the Buranga pegmatite, Rwanda, was solved by Moore (1971), who proposed the general structural formula $\text{X}_2\text{X}_1\text{M}_1\text{M}_2(\text{PO}_4)_3$ [$a = 12.004(2)$ Å, $b = 12.533(4)$ Å, $c = 6.404(1)$ Å, $\beta = 114.4(1)^\circ$, space group $\text{C}2/c$, $Z = 4$]. The nomenclature of the alluaudite group (Moore and Ito 1979) is based on the occupancy of the M1 and M2 crystallographic sites, and leads to five distinct mineral species: alluaudite [$\text{NaMnFe}_2^+(\text{PO}_4)_3$], ferroalluaudite [$\text{NaFe}^{2+}\text{Fe}_2^+(\text{PO}_4)_3$], hagendorfite [$\text{NaCaMnFe}_2^+(\text{PO}_4)_3$], maghagendorfite [$\text{NaMgMnFe}_2^+(\text{PO}_4)_3$], and varulite [$\text{NaCaMnMn}_2(\text{PO}_4)_3$].

Over the past 20 years, many synthetic alluaudite-type phosphates, arsenates, and molybdates have been reported (see Keller et al. 1981; Riffel et al. 1985; Keller and Hess 1988; Auernhammer et al. 1993; Solodovnikov et al. 1998; Hatert et al. 2000; Tsyrenova et al. 2000; Hatert 2004, 2008; Redhammer et al. 2005). A good knowledge of the crystal chemistry of these compounds is necessary because alluaudite-type phosphates are potential materials for practical applications, such as corrosion inhibition, passivation of metal surfaces, catalysis, and energy storage (Korzynski et al. 1998; Richardson 2003; Kacimi et al. 2005). With this goal in mind, Hatert et al. (2000, 2002) and Hatert (2004) investigated in detail the crystal chemistry of lithium in synthetic alluaudite-type phosphates, while the role of the trivalent cation was deciphered by Antenucci (1992) and

Hatert et al. (2003). Starting from these studies, Hatert et al. (2000) proposed a new structural formula, $[\text{A}_2\text{A}'_2][\text{A}_1\text{A}'_1\text{A}''_1]\text{M}_1\text{M}_2[\text{PO}_4]_3$, for alluaudite-type phosphates. Extensive Mössbauer spectral investigations have also been realized (Hermann et al. 2002; Hatert et al. 2003, 2004, 2005; Redhammer et al. 2005), showing the existence of next-nearest neighbor interactions affecting the iron atoms localized on the M sites.

Alluaudite-type phosphates also play a crucial role in our understanding of granitic pegmatite evolution processes. Since the petrogenetic significance of accessory phosphates has been demonstrated in the ultrahigh-pressure rocks of the Dora-Maira massif (Brunet et al. 1998), it now clearly appears that experimental studies on these rare minerals are necessary to better understand the genesis of granitic pegmatites (London et al. 1999, 2001). To assess the geothermometric potential of the $\text{Na}_2(\text{Mn}_{2-2x}\text{Fe}_{1+2x})(\text{PO}_4)_3$ system ($x = 0$ to 1), Hatert et al. (2006) performed systematic hydrothermal experiments between 400 and 800 °C, at 1 kbar and under oxygen fugacities controlled by the Ni-NiO, Fe_2O_3 - Fe_3O_4 , Cu_2O - CuO , and Fe - Fe_3O_4 buffers. These experiments showed that under an oxygen fugacity controlled by the Ni-NiO buffer, single-phase alluaudites crystallize at 400 and 500 °C, whereas the association alluaudite + maričite appears between 500 and 700 °C. The value of alluaudite-type phosphates to estimate the oxygen fugacity conditions that prevailed in granitic pegmatites was also demonstrated (Hatert et al. 2006).

In minerals of the alluaudite group, divalent cations Mg (0.39–5.06 wt% MgO), Ca (0.86–2.20 wt% CaO), and Zn (0.00–0.23 wt% ZnO) play a significant crystal-chemical role, as shown by Moore and Ito (1979). Since the presence of these minor cations affects the stability field of alluaudite-type

* E-mail: fhatert@ulg.ac.be

phosphates, Hatert (2008) performed solid-state synthesis that allowed to decipher the role of Zn and Cd in the $\text{Na}_{1.5}(\text{Mn}_{1-x}\text{M}^{2+})_{1.5}\text{Fe}_{1.5}(\text{PO}_4)_3$ ($M^{2+} = \text{Cd}, \text{Zn}$) solid solutions. Because the oxidized compositions investigated by this author do not correspond to those observed in pegmatites, we decided to hydrothermally synthesize the $\text{Na}_2(\text{Mn}_{1-x}\text{M}^{2+})\text{Fe}^{2+}\text{Fe}^{3+}(\text{PO}_4)_3$ ($x = 0$ to 1, $M^{2+} = \text{Mg}, \text{Cd}, \text{Ca}, \text{Ni}, \text{Zn}$) solid solutions, which better correspond to the natural compositions of alluaudite-type phosphates since they contain a significant amount of Fe^{2+} . The results of the structural and infrared spectral investigations of these compounds are given in the present paper.

EXPERIMENTAL METHODS

Compounds of $\text{Na}_2(\text{Mn}_{1-x}\text{M}^{2+})\text{Fe}^{2+}\text{Fe}^{3+}(\text{PO}_4)_3$ ($x = 0$ to 1, $M^{2+} = \text{Mg}, \text{Cd}, \text{Ca}, \text{Ni}, \text{Zn}$) solid solutions were synthesized under hydrothermal conditions at 1 kbar, between 400 and 600 °C. Stoichiometric quantities of $\text{NaH}_2\text{PO}_4 \cdot \text{H}_2\text{O}$ (Merck, Darmstadt, Germany, min. 99%), MnO (Alfa, Karlsruhe, Germany, 99.5%), MgO (UCB, Leuven, Belgium, min. 94.5%), FeO (Aldrich, Steinheim, Germany, 99%), Fe_2O_3 (Acros, Geel, Belgium, 99.999%), FePO_4 , $\text{Ca}_3(\text{PO}_4)_2$, CdO (UCB, Leuven, Belgium), ZnO (Merck, Darmstadt, Germany, min. 99%), and NiO (Acros, Geel, Belgium) were homogenized in a mortar under acetone, to prevent oxidation of FeO . FePO_4 and $\text{Ca}_3(\text{PO}_4)_2$ were previously synthesized by solid-state reaction in air, starting from stoichiometric mixtures of $\text{NH}_4\text{H}_2\text{PO}_4$ (Merck, Darmstadt, Germany, min. 99%) + Fe_2O_3 , and of CaCO_3 (Merck, Darmstadt, Germany, min. 99%) + $\text{NH}_4\text{H}_2\text{PO}_4$, which were heated in a platinum crucible at 950 °C for 1 day.

Approximately 100 mg of the starting material were welded, together with 10 μL of distilled water, into silver tubes with an outer diameter of 4 mm and a length of 40 mm. The closed silver capsules were finally introduced in a conventional hydrothermal apparatus with vertically arranged Tuttle-type cold-seal vessels (Tuttle 1949) for seven days and then cooled in a stream of cold air. Pressure and temperature errors are estimated to be within around 3% and 10 °C, respectively.

The X-ray powder diffraction patterns of the compounds were recorded with a Phillips PW-3710 diffractometer using $\text{FeK}\alpha$ radiation ($\lambda = 1.9373 \text{ \AA}$). The unit-cell parameters (Table 1) were calculated with the LCLSQ 8.4 least-squares refinement program (Burnham 1991), using the d -spacings corrected with an internal standard of $\text{Pb}(\text{NO}_3)_2$. These unit-cell parameters, as well as the atomic positions reported for synthetic $\text{Na}_2\text{MnFe}^{2+}\text{Fe}^{3+}(\text{PO}_4)_3$ (Hatert et al. 2005), served as starting parameters for the Rietveld refinements that were performed with the DBWS-9807 program (Young et al. 1998). The investigated 2θ range extended from 10 to 100° with step size of 0.02° and a step time of 15 s. Experimental details for the Rietveld refinements are given in Table 2, and the final Rietveld plot for $\text{Na}_2\text{CdFe}^{2+}\text{Fe}^{3+}(\text{PO}_4)_3$ is shown in Figure 1. Fits of equivalent quality were obtained for the other compounds.

The wet chemical analyses (Table 3) were performed using 59 to 124 mg of material. Sodium, Mn, Fe, Cd, and Mg were determined with an Analytic Jena Novaa 300 atomic absorption spectrophotometer, whereas P was measured by colorimetry. The amounts of FeO and Fe_2O_3 were calculated to maintain charge balance.

The infrared spectra were recorded with a Nicolet NEXUS spectrometer, over 400–4000 cm^{-1} region, from 32 scans with 1 cm^{-1} resolution. The samples were prepared by intimately mixing 2 mg of sample with 148 mg of KBr to obtain a 150 mg homogeneous pellet, which was subsequently dried for a few hours at 110 °C. To prevent water contamination, the measurements were performed under a dry air purge.

RESULTS AND DISCUSSION

Mineralogical characterization of the compounds

The $\text{Na}_2(\text{Mn}_{1-x}\text{M}^{2+})\text{Fe}^{2+}\text{Fe}^{3+}(\text{PO}_4)_3$ ($M^{2+} = \text{Mg}, \text{Cd}, \text{Ca}, \text{Ni}$, and Zn) alluaudite-type compounds crystallize in fine-grained light green to olive green powders. The X-ray powder diffraction patterns indicate that pure alluaudites are obtained for the $\text{Na}_2(\text{Mn}_{1-x}\text{Cd}^{2+})\text{Fe}^{2+}\text{Fe}^{3+}(\text{PO}_4)_3$ ($x = 0$ to 1), $\text{Na}_2(\text{Mn}_{1-x}\text{Mg}^{2+})\text{Fe}^{2+}\text{Fe}^{3+}(\text{PO}_4)_3$ ($x = 0$ to 0.75), and $\text{Na}_2(\text{Mn}_{1-x}\text{Ni}^{2+})\text{Fe}^{2+}\text{Fe}^{3+}(\text{PO}_4)_3$ ($x = 0.25, 0.75, 1$) solid solutions, whereas the $\text{Na}_2(\text{Mn}_{1-x}\text{M}^{2+})\text{Fe}^{2+}\text{Fe}^{3+}(\text{PO}_4)_3$ ($M^{2+} = \text{Ca}, \text{Zn}$) solid solutions show significant

TABLE 1. Unit-cell parameters for the $\text{Na}_2(\text{Mn}_{1-x}\text{M}^{2+})\text{Fe}^{2+}\text{Fe}^{3+}(\text{PO}_4)_3$ ($M^{2+} = \text{Cd}, \text{Ca}, \text{Mg}, \text{Zn}, \text{Ni}$) alluaudite-type compounds

Solid solution	x	a (Å)	b (Å)	c (Å)	β (°)	V (Å ³)
$\text{Na}_2(\text{Mn}_{1-x}\text{Cd}_x)\text{Fe}^{2+}\text{Fe}^{3+}(\text{PO}_4)_3$	0.25	12.020(2)	12.578(3)	6.477(1)	114.40(2)	891.7(2)
	0.50	12.058(2)	12.585(2)	6.488(1)	114.39(1)	896.7(2)
	0.75	12.101(4)	12.605(3)	6.496(1)	114.43(2)	902.1(3)
	1.00	12.144(2)	12.612(2)	6.490(1)	114.38(1)	905.4(2)
$\text{Na}_2(\text{Mn}_{1-x}\text{Ca}_x)\text{Fe}^{2+}\text{Fe}^{3+}(\text{PO}_4)_3$	0.25	12.051(4)	12.588(3)	6.480(1)	114.54(2)	894.4(3)
	0.50	12.143(3)	12.621(2)	6.485(1)	114.62(2)	903.5(2)
	0.75	12.198(3)	12.654(3)	6.481(1)	114.68(2)	909.0(2)
	1.00	12.196(3)	12.695(3)	6.508(1)	114.77(2)	914.9(2)
$\text{Na}_2(\text{Mn}_{1-x}\text{Mg}_x)\text{Fe}^{2+}\text{Fe}^{3+}(\text{PO}_4)_3$	0.25	11.943(3)	12.528(2)	6.454(1)	114.22(2)	880.6(2)
	0.50	11.926(3)	12.503(2)	6.440(2)	114.15(2)	876.3(3)
	0.75	11.868(2)	12.486(2)	6.429(1)	114.07(1)	869.9(2)
	1.00	11.793(2)	12.476(2)	6.467(1)	114.29(1)	867.3(2)
$\text{Na}_2(\text{Mn}_{1-x}\text{Zn}_x)\text{Fe}^{2+}\text{Fe}^{3+}(\text{PO}_4)_3$	0.25	11.930(2)	12.551(2)	6.474(1)	114.31(1)	883.4(2)
	0.50	11.889(2)	12.538(2)	6.460(1)	114.18(1)	878.4(2)
	0.75	11.840(3)	12.519(3)	6.449(1)	114.10(2)	872.6(2)
	1.00	11.833(2)	12.494(2)	6.441(1)	113.97(1)	870.0(2)
$\text{Na}_2(\text{Mn}_{1-x}\text{Ni}_x)\text{Fe}^{2+}\text{Fe}^{3+}(\text{PO}_4)_3$	0.25	11.927(3)	12.507(3)	6.465(2)	114.27(2)	879.1(3)
	0.50	11.971(2)	12.453(2)	6.424(1)	113.93(2)	875.4(2)
	0.75	11.817(6)	12.422(6)	6.454(3)	114.20(5)	864.1(6)
	1.00	11.800(4)	12.414(3)	6.434(2)	113.82(3)	862.2(3)

TABLE 2. Experimental details for the Rietveld refinement of the $\text{Na}_2(\text{Mn}_{1-x}\text{M}^{2+})\text{Fe}^{2+}\text{Fe}^{3+}(\text{PO}_4)_3$ ($M^{2+} = \text{Mg}, \text{Cd}$) alluaudite-type phosphates

	H.133	H.181	H.183	H.185	H.173	AH.3	AH.2	AH.1
Number of reflections	500	504	504	504	507	500	498	498
Refined parameters	50	49	49	49	49	50	49	47
Positional	27	27	27	27	27	27	27	27
Population	4	3	3	3	3	4	3	4
Thermal	1	2	2	2	2	1	2	0
Cell parameters	4	4	4	4	4	4	4	4
Background	5	5	5	5	5	5	5	5
Profile	5	4	4	4	4	5	4	4
Zero point (°2 θ)	1	1	1	1	1	1	1	1
Sample displacement	1	1	1	1	1	1	1	1
Scale factor	1	1	1	1	1	1	1	1
Preferred orientation	1	1	1	1	1	1	1	0
R_p (%)	2.14	2.52	2.80	2.65	3.21	2.11	2.52	2.43
R_{wp} (%)	2.93	3.57	3.78	3.43	4.26	2.86	3.41	3.32
R_{exp} (%)	1.46	1.74	1.91	2.24	2.27	1.53	1.63	1.68
S (GooF)	2.00	2.04	1.96	1.52	1.87	1.86	2.08	1.96
R_{Bragg} (%)	5.61	6.17	6.50	4.64	5.83	5.03	6.86	5.93

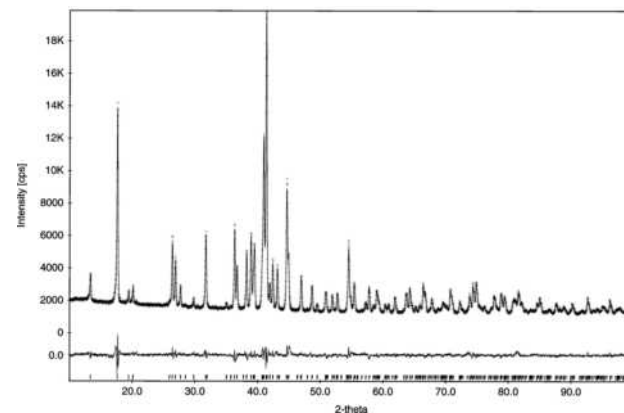


FIGURE 1. The observed (crosses), calculated (solid line), and difference X-ray powder diffraction patterns of $\text{Na}_2\text{CdFe}^{2+}\text{Fe}^{3+}(\text{PO}_4)_3$, obtained from a Rietveld refinement. The vertical markers indicate the calculated positions of the $\text{FeK}\alpha_1$ and $\text{FeK}\alpha_2$ Bragg reflections.

TABLE 3. Wet chemical analyses of the synthetic $\text{Na}_2(\text{Mn}_{1-x}\text{M}^{2+})\text{Fe}^{2+}\text{Fe}^{3+}(\text{PO}_4)_3$ ($M^{2+} = \text{Mg}, \text{Cd}$) alluaudite-type compounds

	H.133*	H.181	H.183	H.185	H.173	AH.3	AH.2	AH.1
P ₂ O ₅	42.52	41.23	38.44	37.92	37.17	41.71	42.42	42.28
Fe ₂ O ₃	20.38	26.30	15.31	14.48	12.90	20.86	23.86	19.44
FeO	10.27	2.58	13.09	13.37	14.31	9.30	7.94	12.47
MgO	—	—	—	—	—	1.35	2.67	4.76
MnO	13.52	8.65	5.65	2.67	0.00	9.53	6.46	3.31
CdO	—	6.38	12.38	18.51	24.03	—	—	—
Na ₂ O	12.44	10.52	10.33	10.02	9.73	11.92	11.19	11.78
Total	99.13	95.66	95.20	96.97	98.14	94.67	94.54	94.04
Cation numbers								
P	3.000	3.000	3.000	3.000	3.000	3.000	3.000	3.000
Fe ³⁺	1.278	1.701	1.062	1.018	0.925	1.334	1.500	1.226
Fe ²⁺	0.716	0.185	1.009	1.045	1.141	0.661	0.554	0.874
Mg	—	—	—	—	—	0.171	0.332	0.595
Mn	0.954	0.630	0.441	0.211	0.000	0.686	0.457	0.235
Cd	—	0.257	0.534	0.809	1.072	—	—	—
Na	2.010	1.753	1.846	1.815	1.799	1.964	1.812	1.914

Notes: Analyst B. Belot. The cation numbers were calculated on the basis of 3 P per formula unit. The amounts of FeO and Fe₂O₃ were calculated to maintain charge balance.

* Data from Hatert et al. (2005).

amounts of impurities (Table 4). The presence of these impurities, and the poor quality of the Rietveld refinements realized on the Ni-bearing phosphates, forced us to focus our study on the $\text{Na}_2(\text{Mn}_{1-x}\text{M}^{2+})\text{Fe}^{2+}\text{Fe}^{3+}(\text{PO}_4)_3$ ($M^{2+} = \text{Cd}, \text{Mg}$) compounds.

The wet chemical analyses of the $\text{Na}_2(\text{Mn}_{1-x}\text{M}^{2+})\text{Fe}^{2+}\text{Fe}^{3+}(\text{PO}_4)_3$ ($M^{2+} = \text{Cd}, \text{Mg}$) compounds (Table 3) show chemical compositions fairly close to the starting compositions. The calculated Fe²⁺ contents, which generally range between 8 and 14 wt% FeO, are in good agreement with the value 10.27 wt% FeO obtained by Hatert et al. (2005) for $\text{Na}_2\text{MnFe}^{2+}\text{Fe}^{3+}(\text{PO}_4)_3$. The totals of the analyses are generally low (ca. 94–98 wt%), suggesting the presence of H₂O that was, however, not detected by the infrared spectral analysis (see below). The presence of H₂O in alluaudite-type phosphates was previously reported by Lii and Shih (1994), Leroux et al. (1995a, 1995b), and Guesmi and Driss (2002).

Structure refinements

The positional parameters, site occupancies, isotropic temperature factors, and interatomic distances and angles, deduced from the Rietveld refinements of the powder X-ray diffraction patterns of the $\text{Na}_2(\text{Mn}_{1-x}\text{Cd}_x)\text{Fe}^{2+}\text{Fe}^{3+}(\text{PO}_4)_3$ ($x = 0.00, 0.25, 0.50, 0.75$, and 1.00) and $\text{Na}_2(\text{Mn}_{1-x}\text{Mg}_x)\text{Fe}^{2+}\text{Fe}^{3+}(\text{PO}_4)_3$ ($x = 0.00, 0.25, 0.50$, and 0.75) alluaudite-type compounds, are presented in Tables 5 to 8. The satisfactory R_p , R_{wp} , R_{Bragg} , and S values (Table 2), as well as the mean P-O distances and O-P-O angles (Tables 7 and 8), confirm the reliability of the refinements. A polyhedral representation of the crystal structure of $\text{Na}_2\text{CdFe}^{2+}\text{Fe}^{3+}(\text{PO}_4)_3$, approximately projected along [001], is shown in Figure 2.

The positional parameters of the alluaudite-type compounds (Tables 5 and 6) correspond to the A2', A1, M1, and M2 crystallographic sites, and the coordination polyhedra morphologies of M1 (very distorted octahedron), M2 (distorted octahedron), A1 (distorted cube), and A2' (gable disphenoid), are similar to those previously described for many synthetic alluaudite-type phosphates (Antenucci et al. 1993, 1995; Hatert et al. 2000, 2003, 2005; Hatert 2004, 2008; Redhammer et al. 2005).

The M1 and M2 site occupancy factors for $\text{Na}_2(\text{Mn}_{1-x}\text{Cd}_x)\text{Fe}^{2+}\text{Fe}^{3+}(\text{PO}_4)_3$ (Table 5) were constrained with the Mn contents

obtained by the wet chemical analyses (Table 3). All iron was considered to be located in the M2 site, and Mn was considered to be located in M1, according to the previous crystal-chemical investigations of alluaudite-type phosphates [see Hatert (2004, 2008) and Redhammer et al. (2005) for recent references]. The number of electrons occurring in the M sites indicates that the replacement of Mn by Cd takes place on the M1 site, but pre-

TABLE 4. Results of synthesis experiments on the $\text{Na}_2(\text{Mn}_{1-x}\text{M}^{2+})\text{Fe}^{2+}\text{Fe}^{3+}(\text{PO}_4)_3$ ($M^{2+} = \text{Cd}, \text{Ca}, \text{Mg}, \text{Zn}, \text{Ni}$) solid solutions

Solid solution	x	T (°C)	Synthesized compounds	Run no.
$\text{Na}_2(\text{Mn}_{1-x}\text{Cd}_x)$	0.25	400	Alluaudite + ?? (tr.)	H.181
$\text{Fe}^{2+}\text{Fe}^{3+}(\text{PO}_4)_3$	0.50	400	Alluaudite + ?? (tr.)	H.183
	0.75	400	Alluaudite + ?? (tr.)	H.185
	1.00	400	Alluaudite	H.173
	1.00	600	Alluaudite	H.174
$\text{Na}_2(\text{Mn}_{1-x}\text{Ca}_x)$	0.25	500	Alluaudite + ?? (tr.)	H.188
$\text{Fe}^{2+}\text{Fe}^{3+}(\text{PO}_4)_3$	0.50	500	Alluaudite + ??	H.190
	0.75	500	Alluaudite + ??	H.192
	1.00	400	Poorly crystallized alluaudite + ??	H.171
	1.00	600	Alluaudite + ??	H.172
$\text{Na}_2(\text{Mn}_{1-x}\text{Mg}_x)$	0.25	600	Alluaudite + ?? (tr.)	H.182
$\text{Fe}^{2+}\text{Fe}^{3+}(\text{PO}_4)_3$	0.25	400	Alluaudite	AH.3
	0.50	600	Alluaudite + ?? (tr.)	H.184
	0.50	400	Alluaudite	AH.2
	0.75	600	Alluaudite + Mg(H ₂ PO ₄) ₂ (tr.)	H.186
	0.75	400	Alluaudite	AH.1
	1.00	400	Alluaudite + ??	H.169
	1.00	600	Alluaudite + Mg(H ₂ PO ₄) ₂	H.170
$\text{Na}_2(\text{Mn}_{1-x}\text{Zn}_x)$	0.25	400	Alluaudite + β-NaZnPO ₄ (tr.)	H.187
$\text{Fe}^{2+}\text{Fe}^{3+}(\text{PO}_4)_3$	0.50	400	Alluaudite + ??	H.189
	0.75	400	Alluaudite + ??	H.191
	1.00	400	Alluaudite + β-NaZnPO ₄	H.175
	1.00	600	Alluaudite + ??	H.176
$\text{Na}_2(\text{Mn}_{1-x}\text{Ni}_x)$	0.25	400	Alluaudite + ?? (tr.)	H.193
$\text{Fe}^{2+}\text{Fe}^{3+}(\text{PO}_4)_3$	0.25	600	Alluaudite + ?? (tr.)	AH.6
	0.50	400	Alluaudite + ??	H.195
	0.50	600	Alluaudite + ??	AH.5
	0.75	400	Alluaudite + ??	H.197
	0.75	600	Alluaudite	AH.4
	1.00	400	Alluaudite + ?? (tr.)	H.177
	1.00	600	Alluaudite	H.178

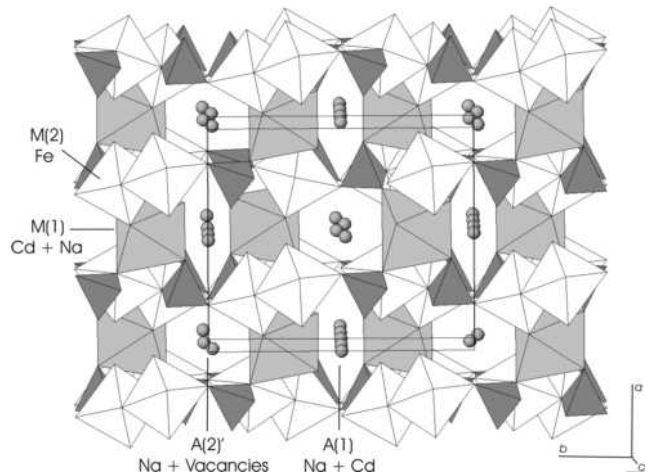


FIGURE 2. Projection of the crystal structure of $\text{Na}_2\text{CdFe}^{2+}\text{Fe}^{3+}(\text{PO}_4)_3$ along the c axis. The PO_4 tetrahedra are densely shaded. The shaded M1 octahedra are occupied by Cd and Na, and the unshaded M2 octahedra are occupied by Fe. The circles indicate the A1 and A2' crystallographic sites.

TABLE 5. Positional (x,y,z), isotropic thermal (B) and site occupancy (N) parameters for the $\text{Na}_2(\text{Mn}_{1-x}\text{Cd}_x)\text{Fe}^{2+}\text{Fe}^{3+}(\text{PO}_4)_3$ alluaudite-type compounds

Site	Atom	Wyckoff	x	y	z	B (Å ²)	N
$\text{Na}_2\text{MnFe}^{2+}\text{Fe}^{3+}(\text{PO}_4)_3$ (x = 0.00, H.133)							
A2'	Na	4e	0	-0.0113(7)	1/4	1.0*	0.379(6)
A1	Na	4b	1/2	0	0	1.0*	0.481(6)
M1	Mn	4e	0	0.2690(3)	1/4	1.0*	0.500
M2	Fe	8f	0.2795(3)	0.6573(2)	0.3641(5)	1.0*	0.984(5)
P1	P	4e	0	-0.2846(5)	1/4	1.0*	0.5
P2	P	8f	0.2370(4)	-0.1106(3)	0.1238(9)	1.0*	1.0
O1	O	8f	0.4584(7)	0.7139(6)	0.538(1)	1.1(1)	1.0
O2	O	8f	0.1027(8)	0.6433(5)	0.239(1)	1.1(1)	1.0
O3	O	8f	0.3365(7)	0.6703(5)	0.110(1)	1.1(1)	1.0
O4	O	8f	0.1270(7)	0.3992(5)	0.328(1)	1.1(1)	1.0
O5	O	8f	0.2283(6)	0.8256(6)	0.326(1)	1.1(1)	1.0
O6	O	8f	0.3235(6)	0.4947(7)	0.384(1)	1.1(1)	1.0
$\text{Na}_2\text{Cd}_{0.25}\text{Mn}_{0.75}\text{Fe}^{2+}\text{Fe}^{3+}(\text{PO}_4)_3$ (x = 0.25, H.181)							
A2'	Na	4e	0	-0.0092(9)	1/4	1.0*	0.366(7)
A1	Na	4b	1/2	0	0	1.0*	0.480(2)
	Cd	4b	1/2	0	0	1.0*	0.020(2)
M1	Cd	4e	0	0.2682(3)	1/4	1.0*	0.116(3)
	Na	4e	0	0.2682(3)	1/4	1.0*	0.069(3)
	Mn	4e	0	0.2682(3)	1/4	1.0*	0.315
M2	Fe	8f	0.2791(3)	0.6578(2)	0.3642(6)	1.0*	1.0
P1	P	4e	0	-0.2827(5)	1/4	0.1(2)	0.5
P2	P	8f	0.2375(5)	-0.1069(4)	0.1288(9)	0.1(2)	1.0
O1	O	8f	0.4558(8)	0.7112(7)	0.539(1)	0.9(1)	1.0
O2	O	8f	0.0982(8)	0.6418(6)	0.235(1)	0.9(1)	1.0
O3	O	8f	0.3268(8)	0.6600(7)	0.101(1)	0.9(1)	1.0
O4	O	8f	0.1303(7)	0.4064(6)	0.332(1)	0.9(1)	1.0
O5	O	8f	0.2300(7)	0.8238(7)	0.324(2)	0.9(1)	1.0
O6	O	8f	0.3211(5)	0.5002(8)	0.380(1)	0.9(1)	1.0
$\text{Na}_2\text{Cd}_{0.5}\text{Mn}_{0.5}\text{Fe}^{2+}\text{Fe}^{3+}(\text{PO}_4)_3$ (x = 0.50, H.183)							
A2'	Na	4e	0	-0.0103(7)	1/4	1.0*	0.408(6)
A1	Na	4b	1/2	0	0	1.0*	0.466(2)
	Cd	4b	1/2	0	0	1.0*	0.034(2)
M1	Cd	4e	0	0.2694(2)	1/4	1.0*	0.200(3)
	Na	4e	0	0.2694(2)	1/4	1.0*	0.080(3)
	Mn	4e	0	0.2694(2)	1/4	1.0*	0.220
M2	Fe	8f	0.2789(3)	0.6578(2)	0.3637(6)	1.0*	1.0
P1	P	4e	0	-0.2797(5)	1/4	0.1(1)	0.5
P2	P	8f	0.2373(4)	-0.1036(3)	0.1310(9)	0.1(1)	1.0
O1	O	8f	0.4588(7)	0.7060(6)	0.542(1)	0.9(1)	1.0
O2	O	8f	0.0890(7)	0.6419(6)	0.226(1)	0.9(1)	1.0
O3	O	8f	0.3189(7)	0.6545(6)	0.096(1)	0.9(1)	1.0
O4	O	8f	0.1305(6)	0.4108(5)	0.328(1)	0.9(1)	1.0
O5	O	8f	0.2346(7)	0.8227(6)	0.327(2)	0.9(1)	1.0
O6	O	8f	0.3197(5)	0.5052(7)	0.382(1)	0.9(1)	1.0

liminary refinement cycles show unexpectedly high electronic densities on A1 and very low electronic densities on M1. These features indicate that small amounts of Cd occur on the A1 site, compensated by small amounts of Na on M1. In the final refinement cycle, Na against Cd were consequently refined on both A1 and M1 sites (Table 5). This partially disordered distribution is certainly due to the similar effective ionic radii of Cd and Na, which are 0.95 and 1.02 Å, respectively (Shannon 1976). As shown in Figure 3, the M1 site is able to accommodate a maximal amount of 0.33 Na apfu, an amount that is close to the 0.35 Na apfu. observed in the M1 site of $\text{Na}_{1.70}\text{Mn}_{0.65}\text{Fe}_3^{2+}(\text{PO}_4)_3$. This last value probably corresponds to the maximal Na content of the M1 site in alluaudite-type phosphates (Hatert 2002). Figure 3 also shows that the amount of Cd occurring in the A1 site increases linearly when x increases, thus indicating that larger amounts of Cd could be inserted in A1. This observation is in good agreement with the structural data obtained on $\text{NaCaCdMg}_2(\text{PO}_4)_3$, in which the A1 site is able to incorporate more than 50 mol% Cd (Antenucci et al. 1995).

The significant increase of the M1-O bond lengths con-

TABLE 5.—CONTINUED

Site	Atom	Wyckoff	x	y	z	B (Å ²)	N
$\text{Na}_2\text{Cd}_{0.75}\text{Mn}_{0.25}\text{Fe}^{2+}\text{Fe}^{3+}(\text{PO}_4)_3$ (x = 0.75, H.185)							
A2'	Na	4e	0	-0.0130(8)	1/4	1.0*	0.380(6)
A1	Na	4b	1/2	0	0	1.0*	0.455(2)
	Cd	4b	1/2	0	0	1.0*	0.045(2)
M1	Cd	4e	0	0.2686(2)	1/4	1.0*	0.319(3)
	Na	4e	0	0.2686(2)	1/4	1.0*	0.075(3)
	Mn	4e	0	0.2686(2)	1/4	1.0*	0.106
M2	Fe	8f	0.2769(3)	0.6572(2)	0.3616(5)	1.0*	1.0
P1	P	4e	0	-0.2790(4)	1/4	0.6(1)	0.5
P2	P	8f	0.2384(4)	-0.1044(3)	0.1320(8)	0.6(1)	1.0
O1	O	8f	0.4555(6)	0.7052(6)	0.543(1)	1.1(1)	1.0
O2	O	8f	0.0957(6)	0.6443(5)	0.231(1)	1.1(1)	1.0
O3	O	8f	0.3239(6)	0.6579(5)	0.100(1)	1.1(1)	1.0
O4	O	8f	0.1283(6)	0.4105(5)	0.324(1)	1.1(1)	1.0
O5	O	8f	0.2328(6)	0.8251(6)	0.328(1)	1.1(1)	1.0
O6	O	8f	0.3243(5)	0.5026(6)	0.3843(9)	1.1(1)	1.0
$\text{Na}_2\text{CdFe}^{2+}\text{Fe}^{3+}(\text{PO}_4)_3$ (x = 1.00, H.173)							
A2'	Na	4e	0	-0.0125(8)	1/4	1.0*	0.376(7)
A1	Na	4b	1/2	0	0	1.0*	0.453(2)
	Cd	4b	1/2	0	0	1.0*	0.047(2)
M1	Cd	4e	0	0.2689(2)	1/4	1.0*	0.335(4)
	Na	4e	0	0.2689(2)	1/4	1.0*	0.165(4)
M2	Fe	8f	0.2758(3)	0.6569(2)	0.3598(5)	1.0*	1.0
P1	P	4e	0	-0.2780(5)	1/4	1.5(1)	0.5
P2	P	8f	0.2393(4)	-0.1029(4)	0.1346(9)	1.5(1)	1.0
O1	O	8f	0.4548(8)	0.7040(7)	0.540(1)	1.9(2)	1.0
O2	O	8f	0.0976(7)	0.6456(6)	0.230(1)	1.9(2)	1.0
O3	O	8f	0.3208(7)	0.6568(6)	0.102(1)	1.9(2)	1.0
O4	O	8f	0.1239(7)	0.4143(6)	0.321(1)	1.9(2)	1.0
O5	O	8f	0.2344(7)	0.8251(7)	0.332(2)	1.9(2)	1.0
O6	O	8f	0.3271(6)	0.5029(7)	0.386(1)	1.9(2)	1.0

* B_{iso} were fixed.

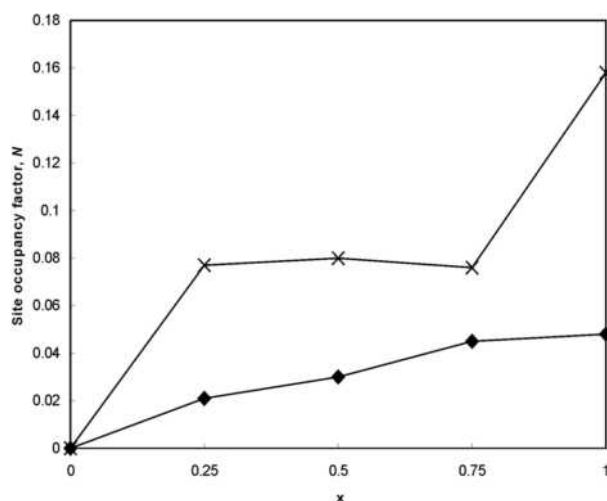


FIGURE 3. Variations of the site occupancy factors of Na on the M1 site (crosses) and of Cd on the A1 site (diamonds), for the $\text{Na}_2(\text{Mn}_{1-x}\text{Cd}_x)\text{Fe}^{2+}\text{Fe}^{3+}(\text{PO}_4)_3$ solid solution.

firms that the insertion of Cd in $\text{Na}_2(\text{Mn}_{1-x}\text{Cd}_x)\text{Fe}^{2+}\text{Fe}^{3+}(\text{PO}_4)_3$ mainly takes place on the M1 site, while the constant M2-O bond lengths indicate that this site is permanently filled by Fe (Table 7). The affinity of Cd for the M1 site was previously demonstrated in the $\text{NaCdIn}_2(\text{PO}_4)_3$, $\text{NaCaCdMg}_2(\text{PO}_4)_3$, and $\text{Na}_{1.5}(\text{Mn}_{1-x}\text{Cd}_x)_{1.5}\text{Fe}_{1.5}(\text{PO}_4)_3$ (x = 0 to 1) alluaudite-type compounds (Antenucci et al. 1993, 1995; Hatert 2008).

Preliminary refinement cycles performed on $\text{Na}_2(\text{Mn}_{1-x}\text{Mg}_x)\text{Fe}^{2+}\text{Fe}^{3+}(\text{PO}_4)_3$ indicate that a Fe-Mg miscibility occurs on the M1 and M2 sites. In the final models, the Mn contents of M1 were constrained to the values obtained from the wet chemi-

TABLE 6. Positional (x, y, z), isotropic thermal (B), and site occupancy (N) parameters for the $\text{Na}_2(\text{Mn}_{1-x}\text{Mg}_x)\text{Fe}^{2+}\text{Fe}^{3+}(\text{PO}_4)_3$ alluaudite-type compounds

Site	Atom	Wyckoff	x	y	z	B (\AA^2)	N
$\text{Na}_2\text{Mg}_{0.25}\text{Mn}_{0.75}\text{Fe}^{2+}\text{Fe}^{3+}(\text{PO}_4)_3$ ($x = 0.25$, AH.3)							
A2'	Na	4e	0	-0.0137(6)	1/4	1.0*	0.390(6)
A1	Na	4b	1/2	0	0	1.0*	0.488(6)
M1	Mn	4e	0	0.2694(3)	1/4	1.0*	0.343
	Fe	4e	0	0.2694(3)	1/4	1.0*	0.110(9)
	Mg	4e	0	0.2694(3)	1/4	1.0*	0.047(9)
M2	Fe	8f	0.2794(3)	0.6578(2)	0.3652(5)	1.0*	0.901(9)
	Mg	8f	0.2794(3)	0.6578(2)	0.3652(5)	1.0*	0.099(9)
P1	P	4e	0	-0.2844(4)	1/4	1.0*	0.5
P2	P	8f	0.2356(4)	-0.1082(3)	0.1267(7)	1.0*	1.0
O1	O	8f	0.4548(6)	0.7139(5)	0.534(1)	0.8(1)	1.0
O2	O	8f	0.1011(7)	0.6389(4)	0.240(1)	0.8(1)	1.0
O3	O	8f	0.3336(6)	0.6657(5)	0.110(1)	0.8(1)	1.0
O4	O	8f	0.1296(6)	0.4013(4)	0.3307(9)	0.8(1)	1.0
O5	O	8f	0.2268(5)	0.8251(5)	0.321(1)	0.8(1)	1.0
O6	O	8f	0.3231(5)	0.5029(6)	0.3825(8)	0.8(1)	1.0
$\text{Na}_2\text{Mg}_{0.5}\text{Mn}_{0.5}\text{Fe}^{2+}\text{Fe}^{3+}(\text{PO}_4)_3$ ($x = 0.50$, AH.2)							
A2'	Na	4e	0	-0.0148(8)	1/4	1.0*	0.397(6)
A1	Na	4b	1/2	0	0	1.0*	0.5
M1	Fe	4e	0	0.2683(3)	1/4	1.0*	0.192(6)
	Mn	4e	0	0.2683(3)	1/4	1.0*	0.229
	Mg	4e	0	0.2683(3)	1/4	1.0*	0.073
M2	Fe	8f	0.2823(3)	0.6563(2)	0.3683(6)	1.0*	0.809(6)
	Mg	8f	0.2823(3)	0.6563(2)	0.3683(6)	1.0*	0.175
P1	P	4e	0	-0.2848(5)	1/4	1.2(1)	0.5
P2	P	8f	0.2399(4)	-0.1068(4)	0.1266(8)	1.2(1)	1.0
O1	O	8f	0.4548(7)	0.7099(6)	0.528(1)	1.1(1)	1.0
O2	O	8f	0.1053(7)	0.6391(5)	0.249(1)	1.1(1)	1.0
O3	O	8f	0.3339(7)	0.6600(6)	0.103(1)	1.1(1)	1.0
O4	O	8f	0.1264(7)	0.4030(6)	0.332(1)	1.1(1)	1.0
O5	O	8f	0.2252(6)	0.8276(6)	0.310(1)	1.1(1)	1.0
O6	O	8f	0.3251(5)	0.5035(8)	0.384(1)	1.1(1)	1.0
$\text{Na}_2\text{Mg}_{0.75}\text{Mn}_{0.25}\text{Fe}^{2+}\text{Fe}^{3+}(\text{PO}_4)_3$ ($x = 0.75$, AH.1)							
A2'	Na	4e	0	-0.0112(9)	1/4	1.0*	0.339(5)
A1	Na	4b	1/2	0	0	1.0*	0.480(3)
M1	Fe	4e	0	0.2682(3)	1/4	1.0*	0.287(6)
	Mn	4e	0	0.2682(3)	1/4	1.0*	0.118
	Mg	4e	0	0.2682(3)	1/4	1.0*	0.095(6)
M2	Fe	8f	0.2830(3)	0.6567(2)	0.3686(6)	1.0*	0.77(1)
	Mg	8f	0.2830(3)	0.6567(2)	0.3686(6)	1.0*	0.23(1)
P1	P	4e	0	-0.2863(5)	1/4	1.0*	0.5
P2	P	8f	0.2385(4)	-0.1113(3)	0.1243(8)	1.0*	1.0
O1	O	8f	0.4572(7)	0.7162(5)	0.530(1)	1.0*	1.0
O2	O	8f	0.1058(8)	0.6423(5)	0.246(1)	1.0*	1.0
O3	O	8f	0.3352(7)	0.6675(6)	0.111(1)	1.0*	1.0
O4	O	8f	0.1265(6)	0.3991(5)	0.330(1)	1.0*	1.0
O5	O	8f	0.2261(6)	0.8261(6)	0.319(1)	1.0*	1.0
O6	O	8f	0.3206(6)	0.4980(8)	0.3832(9)	1.0*	1.0

* B_{iso} were fixed.

cal analyses (Table 3), and Fe against Mg were refined on M1 and M2 (Table 6). In $\text{Na}_2\text{Mn}_{0.5}\text{Mg}_{0.5}\text{Fe}^{2+}\text{Fe}^{3+}(\text{PO}_4)_3$ (AH.2, $x = 0.50$), however, the refinement converged to unacceptable high Mg contents and low Fe contents. We consequently decided to constrain the Mg contents of M1 and M2 to values obtained by extrapolation between those of $\text{Na}_2\text{Mn}_{0.75}\text{Mg}_{0.25}\text{Fe}^{2+}\text{Fe}^{3+}(\text{PO}_4)_3$ (AH.3, $x = 0.25$) and of $\text{Na}_2\text{Mn}_{0.25}\text{Mg}_{0.75}\text{Fe}^{2+}\text{Fe}^{3+}(\text{PO}_4)_3$ (AH.1, $x = 0.75$) (Table 6).

Since the isotropic temperature factors are correlated with the occupancy factors, we decided to constrain the temperature factors to 1.0 for the A2', A1, M1, and M2 sites in all refinements. The isotropic temperature factors were only refined for the O and P atoms (Tables 5 and 6).

Bond valence sums were also calculated for each ion of $\text{Na}_2\text{CdFe}^{2+}\text{Fe}^{3+}(\text{PO}_4)_3$ and $\text{Na}_2\text{Mg}_{0.75}\text{Mn}_{0.25}\text{Fe}^{2+}\text{Fe}^{3+}(\text{PO}_4)_3$, using the empirical parameters of Brown and Altermatt (1985). The P-atoms bond valence sums are between 4.72 and 5.16, and the

TABLE 7. Selected interatomic distances (\AA) and angles ($^\circ$) for the $\text{Na}_2(\text{Mn}_{1-x}\text{Cd}_x)\text{Fe}^{2+}\text{Fe}^{3+}(\text{PO}_4)_3$ alluaudite-type compounds

x	0.00	0.25	0.50	0.75	1.00	Difference
A2'-O6 2x	2.442(6)	2.474(6)	2.479(6)	2.450(5)	2.431(6)	-0.01
A2'-O6 2x	2.593(5)	2.616(4)	2.652(4)	2.618(4)	2.599(5)	0.01
A2'-O1 2x	2.84(1)	2.83(1)	2.75(1)	2.72(1)	2.72(1)	-0.12
A2'-O3 2x	2.893(9)	2.85(1)	2.88(1)	2.901(9)	2.91(1)	0.02
Mean	2.69	2.69	2.69	2.67	2.67	-0.02
A1-O2 2x	2.359(6)	2.325(7)	2.278(7)	2.337(6)	2.355(7)	0.00
A1-O4 2x	2.397(6)	2.383(7)	2.345(6)	2.326(6)	2.277(7)	-0.12
A1-O4 2x	2.559(6)	2.536(6)	2.535(5)	2.541(5)	2.495(6)	-0.06
A1-O2 2x	3.054(6)	3.032(7)	3.013(7)	3.062(6)	3.092(7)	0.04
Mean	2.59	2.57	2.54	2.57	2.55	-0.04
M1-O3 2x	2.169(6)	2.336(8)	2.461(6)	2.392(6)	2.436(7)	0.27
M1-O4 2x	2.143(7)	2.252(7)	2.288(6)	2.285(6)	2.295(7)	0.15
M1-O1 2x	2.231(6)	2.263(8)	2.291(7)	2.324(6)	2.316(8)	0.09
Mean	2.18	2.28	2.35	2.33	2.35	0.17
M2-O3	2.033(6)	2.013(8)	1.986(8)	2.003(7)	1.963(8)	-0.07
M2-O6	2.099(9)	2.04(1)	1.974(9)	2.019(8)	2.025(9)	-0.07
M2-O2	1.930(7)	1.991(7)	2.096(6)	2.004(5)	1.977(6)	0.05
M2-O1	2.084(7)	2.063(8)	2.083(7)	2.078(6)	2.085(7)	0.00
M2-O5	2.060(6)	2.08(1)	2.094(9)	2.080(8)	2.07(1)	0.01
M2-O5	2.186(8)	2.156(9)	2.132(8)	2.171(8)	2.170(9)	-0.02
Mean	2.07	2.06	2.06	2.06	2.05	-0.02
M1-M2	3.327(3)	3.340(3)	3.354(2)	3.377(3)	3.394(3)	0.07
P1-O2 2x	1.550(8)	1.549(8)	1.512(8)	1.552(7)	1.574(7)	0.02
P1-O1 2x	1.535(7)	1.536(9)	1.541(9)	1.538(8)	1.553(9)	0.02
Mean	1.54	1.54	1.53	1.55	1.56	0.02
O2-P1-O2	108.5(5)	104.4(5)	98.6(5)	103.0(5)	104.5(5)	
O1-P1-O1	109.3(5)	108.3(6)	106.0(6)	105.6(5)	106.1(6)	
O2-P1-O1 2x	114.3(3)	114.9(4)	119.8(3)	116.3(3)	115.8(4)	
O2-P1-O1 2x	105.4(3)	107.2(4)	106.8(3)	108.1(3)	107.5(4)	
Mean	109.5	109.5	109.6	109.6	109.5	
P2-O4	1.527(6)	1.511(6)	1.517(6)	1.529(5)	1.580(6)	0.05
P2-O5	1.576(8)	1.57(1)	1.585(9)	1.577(9)	1.59(1)	0.01
P2-O6	1.498(9)	1.51(1)	1.519(9)	1.530(8)	1.536(9)	0.04
P2-O3	1.589(8)	1.52(1)	1.488(8)	1.534(8)	1.56(1)	-0.03
Mean	1.55	1.53	1.53	1.54	1.57	0.02
O4-P2-O3	110.7(4)	106.7(4)	104.0(4)	106.8(3)	105.6(4)	
O6-P2-O3	108.5(4)	108.3(5)	108.8(5)	106.9(4)	106.1(5)	
O6-P2-O5	106.2(4)	110.2(4)	114.4(4)	111.5(4)	111.9(4)	
O5-P2-O3	110.6(4)	111.7(5)	113.0(5)	112.2(4)	112.7(5)	
O6-P2-O4	113.2(4)	110.4(5)	108.7(4)	111.1(4)	111.8(5)	
O4-P2-O5	107.6(4)	109.4(4)	107.3(4)	108.2(4)	108.5(4)	
Mean	109.5	109.5	109.4	109.5	109.4	

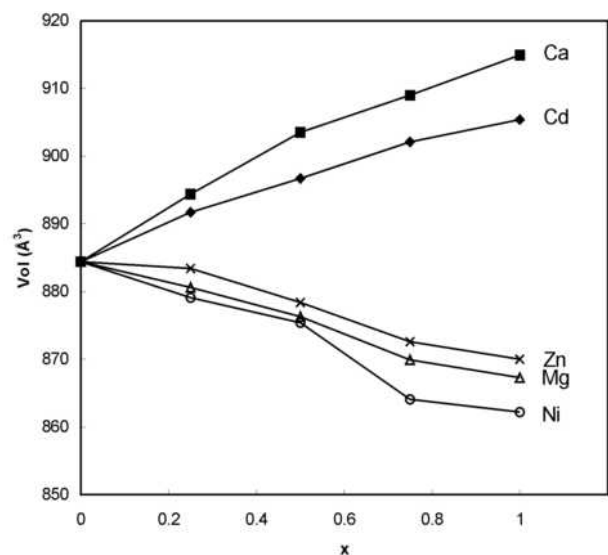
**FIGURE 4.** Correlation between the unit-cell volume and the substitution rate x , for the $\text{Na}_2(\text{Mn}_{1-x}\text{M}^2_x)\text{Fe}^{2+}\text{Fe}^{3+}(\text{PO}_4)_3$ ($\text{M}^2 = \text{Ni, Mg, Zn, Cd, Ca}$) solid solutions.

TABLE 8. Selected interatomic distances (Å) and angles (°) for the $\text{Na}_2(\text{Mn}_{1-x}\text{Mg}_x)\text{Fe}^{2+}\text{Fe}^{3+}(\text{PO}_4)_3$ alluaudite-type compounds

x	0.00	0.25	0.50	0.75	Difference
A2'-O6 2x	2.442(6)	2.449(5)	2.430(5)	2.455(5)	0.01
A2'-O6 2x	2.593(5)	2.592(4)	2.573(4)	2.601(5)	0.01
A2'-O1 2x	2.84(1)	2.812(9)	2.77(1)	2.87(1)	0.03
A2'-O3 2x	2.893(9)	2.889(8)	2.84(1)	2.86(1)	-0.03
Mean	2.69	2.69	2.65	2.70	0.01
A1-O2 2x	2.359(6)	2.313(5)	2.351(6)	2.370(6)	0.01
A1-O4 2x	2.397(6)	2.402(5)	2.383(7)	2.397(6)	0.00
A1-O4 2x	2.559(6)	2.551(5)	2.500(6)	2.525(5)	-0.03
A1-O2 2x	3.054(6)	2.994(6)	2.979(6)	3.012(6)	-0.04
Mean	2.59	2.57	2.55	2.58	-0.01
M1-O3 2x	2.169(6)	2.232(6)	2.263(7)	2.186(7)	0.02
M1-O4 2x	2.143(7)	2.176(6)	2.176(7)	2.135(6)	-0.01
M1-O1 2x	2.231(6)	2.224(6)	2.195(7)	2.160(7)	-0.07
Mean	2.18	2.21	2.21	2.16	-0.02
M2-O3	2.033(6)	2.004(6)	2.040(7)	1.995(7)	-0.04
M2-O6	2.099(9)	2.001(8)	1.97(1)	2.03(1)	-0.07
M2-O2	1.930(7)	1.957(6)	1.940(6)	1.930(7)	0.00
M2-O1	2.084(7)	2.049(6)	2.002(6)	2.038(6)	-0.05
M2-O5	2.060(6)	2.068(7)	2.120(9)	2.066(7)	0.01
M2-O5	2.186(8)	2.173(7)	2.232(8)	2.204(8)	0.02
Mean	2.07	2.04	2.05	2.04	-0.03
M1-M2	3.327(3)	3.325(3)	3.302(3)	3.279(3)	-0.05
P1-O2 2x	1.550(8)	1.565(6)	1.578(7)	1.549(7)	0.00
P1-O1 2x	1.535(7)	1.548(7)	1.607(9)	1.562(8)	0.03
Mean	1.54	1.56	1.59	1.56	0.02
O2-P1-O2	108.5(5)	104.2(4)	105.8(5)	109.7(5)	
O1-P1-O1	109.3(5)	110.4(5)	108.7(5)	111.8(5)	
O2-P1-O1 2x	114.3(3)	113.4(3)	112.2(3)	111.8(3)	
O2-P1-O1 2x	105.4(3)	107.6(3)	109.0(3)	105.9(3)	
Mean	109.5	109.4	109.5	109.5	
P2-O4	1.527(6)	1.523(6)	1.510(6)	1.512(5)	-0.02
P2-O5	1.576(8)	1.546(7)	1.506(9)	1.533(8)	-0.04
P2-O6	1.498(9)	1.549(8)	1.57(1)	1.53(1)	0.03
P2-O3	1.589(8)	1.581(8)	1.529(9)	1.571(9)	-0.02
Mean	1.55	1.55	1.53	1.54	-0.01
O4-P2-O3	110.7(4)	107.8(3)	110.8(4)	110.8(4)	
O6-P2-O3	108.5(4)	108.9(4)	106.2(4)	107.5(4)	
O6-P2-O5	106.2(4)	109.7(3)	107.4(4)	106.6(4)	
O5-P2-O4	110.6(4)	110.8(4)	108.4(5)	111.0(4)	
O6-P2-O4	113.2(4)	111.4(3)	113.8(4)	111.5(4)	
O4-P2-O5	107.6(4)	108.3(3)	111.0(4)	109.4(4)	
Mean	109.5	109.5	109.6	109.5	

O-atoms bond valence sums are within the normally acceptable range (1.85–2.10). The bond valence sums for the cationic sites are in good agreement with the theoretical values, thus confirming the cationic distributions reported in Tables 5 and 6.

Variations of the unit-cell parameters

The unit-cell parameters of the $\text{Na}_2(\text{Mn}_{1-x}\text{M}_x^{2+})\text{Fe}^{2+}\text{Fe}^{3+}(\text{PO}_4)_3$ ($\text{M}^{2+} = \text{Cd}, \text{Ca}, \text{Mg}, \text{Zn}, \text{Ni}$) alluaudite-type compounds show a significant increase when Mn [effective ionic radius 0.830 Å, Shannon (1976)] is replaced by Cd (*e.i.r.* 0.95 Å) or Ca (*e.i.r.* 1.00 Å), and a significant decrease when it is replaced by Ni (*e.i.r.* 0.690 Å), Mg (*e.i.r.* 0.720 Å), or Zn²⁺ (*e.i.r.* 0.740) (Table 1; Fig. 4). The variations of unit-cell parameters for the $\text{Na}_2(\text{Mn}_{1-x}\text{Cd}_x)\text{Fe}^{2+}\text{Fe}^{3+}(\text{PO}_4)_3$ solid solution (Fig. 5a) can also be correlated with variations of the M1-O bond distances (Table 7). In the M1 site, the bond distances most strongly affected by the Mn-Cd substitution are M1-O3 and M1-O4 (Table 7), which are forming a square approximately parallel to the **a-b** plane (Hatert 2008). These strong variations of bond distances are consequently responsible for the more pronounced variations of the *a* and *b* unit-cell parameters, compared to *c* (Fig. 5a). For the $\text{Na}_2(\text{Mn}_{1-x}\text{Mg}_x)\text{Fe}^{2+}\text{Fe}^{3+}(\text{PO}_4)_3$ solid solution, the decrease of the *a* and *b* unit-cell parameters is also more pronounced than the decrease of *c* (Fig. 5b), but this behavior cannot be satisfactorily correlated with the M1-O bond distances, since these distances only show weak variations when the substitution rate increases (Table 8).

Infrared spectral results

The infrared spectra of the $\text{Na}_2(\text{Mn}_{1-x}\text{Cd}_x)\text{Fe}^{2+}\text{Fe}^{3+}(\text{PO}_4)_3$ and $\text{Na}_2(\text{Mn}_{1-x}\text{Mg}_x)\text{Fe}^{2+}\text{Fe}^{3+}(\text{PO}_4)_3$ solid solutions are shown in Figures 6 and 7, respectively, and the assignment of their absorption bands (Table 9) was performed by comparison with those of the $\text{NaMn}(\text{Fe}_{1-x}\text{In}_x)_2(\text{PO}_4)_3$, $\text{Na}_2(\text{Mn}_{1-x}\text{Fe}_x^{2+})_2\text{Fe}^{3+}(\text{PO}_4)_3$, and

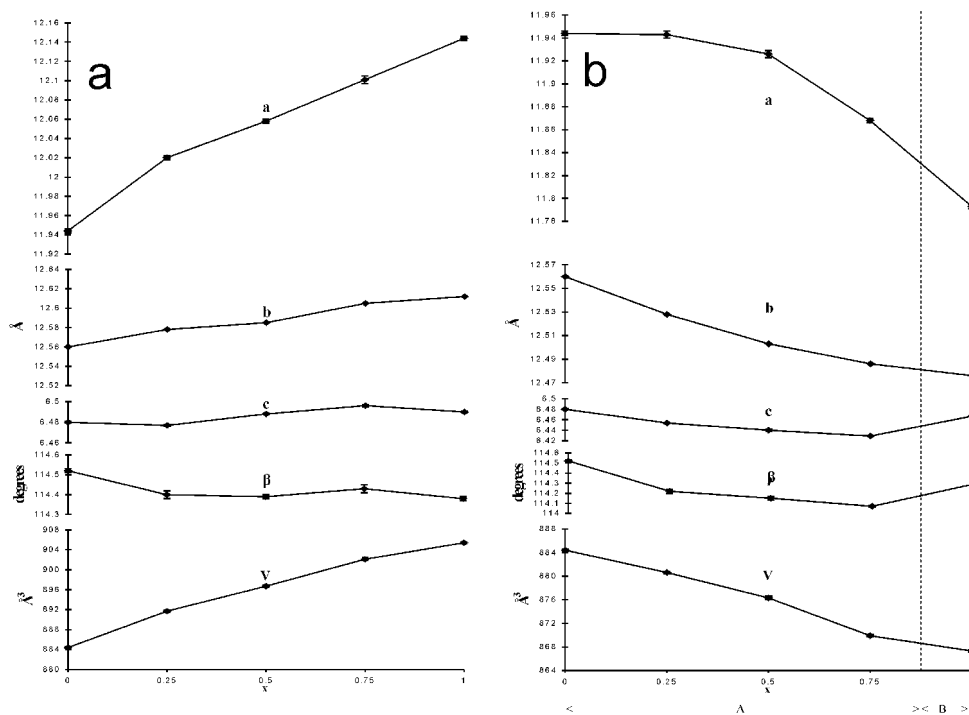


FIGURE 5. The compositional dependence of the unit-cell parameters in (a) $\text{Na}_2(\text{Mn}_{1-x}\text{Cd}_x)\text{Fe}^{2+}\text{Fe}^{3+}(\text{PO}_4)_3$ and (b) $\text{Na}_2(\text{Mn}_{1-x}\text{Mg}_x)\text{Fe}^{2+}\text{Fe}^{3+}(\text{PO}_4)_3$. The error bars are generally smaller than the data points.

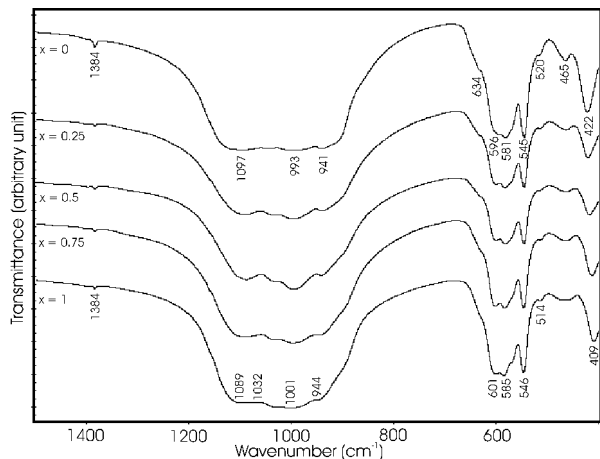


FIGURE 6. Infrared spectra of the $\text{Na}_2(\text{Mn}_{1-x}\text{Cd}_x)\text{Fe}^{2+}\text{Fe}^{3+}(\text{PO}_4)_3$ alluaudite-type compounds.

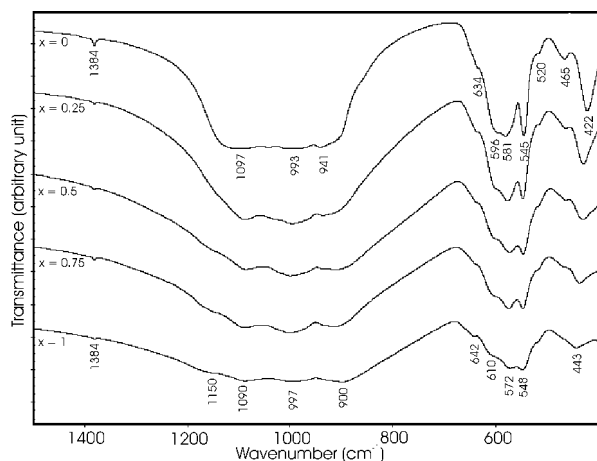


FIGURE 7. Infrared spectra of the $\text{Na}_2(\text{Mn}_{1-x}\text{Mg}_x)\text{Fe}^{2+}\text{Fe}^{3+}(\text{PO}_4)_3$ alluaudite-type compounds.

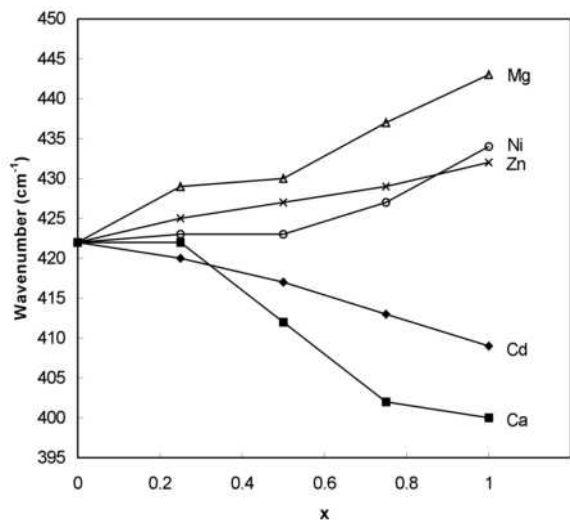


FIGURE 8. Correlation between wavenumber of the infrared absorption band located around 422 cm^{-1} , and the substitution rate x , for the $\text{Na}_2(\text{Mn}_{1-x}\text{M}_x)\text{Fe}^{2+}\text{Fe}^{3+}(\text{PO}_4)_3$ ($M^{2+} = \text{Ni, Mg, Zn, Cd, Ca}$) solid solutions.

$\text{Na}_{1.5}(\text{Mn}_{1-x}\text{M}_x^{2+})_{1.5}\text{Fe}_{1.5}(\text{PO}_4)_3$ ($M^{2+} = \text{Cd, Zn}$) alluaudite-type compounds (Hatert et al. 2003, 2005; Hatert 2008). Infrared spectra and band assignments for the $\text{Na}_2(\text{Mn}_{1-x}\text{M}_x^{2+})\text{Fe}^{2+}\text{Fe}^{3+}(\text{PO}_4)_3$ ($M^{2+} = \text{Ca, Zn, Ni}$) solid solutions are available on deposit¹.

According to the fundamental vibrational frequencies of the PO_4 tetrahedron (Farmer 1974), the absorption bands between 924 and 1384 cm^{-1} can be assigned to ν_3 , the antisymmetric stretching modes of the PO_4 anions, and the bands between 514 and 585 cm^{-1} can be assigned to ν_4 , their bending mode. The weak bands between 900 and 911 cm^{-1} probably correspond to ν_1 , the symmetric stretching mode of the distorted PO_4 tetrahedron (Table 9).

When Mn is replaced by other divalent cations, the infrared spectra show an important displacement of an absorption band found at 422 cm^{-1} , in the spectrum of $\text{Na}_2\text{MnFe}^{2+}\text{Fe}^{3+}(\text{PO}_4)_3$ (Table 9). This band, which shifts toward high wavenumbers when Mn is replaced by smaller cations (Zn, Ni, Mg) and toward low wavenumbers when Mn is replaced by larger cations (Cd, Ca) (Fig. 8), can be assigned to the vibrations of the M^{2+} cations localized on the M1 site, an assignment that is confirmed by the excellent correlation between the average ionic radii of M1 cations and the wavenumber of the absorption band (Fig. 9).

¹ Deposit item AM-10-032, Supplemental table. Deposit items are available two ways: For a paper copy contact the Business Office of the Mineralogical Society of America (see inside front cover of recent issue) for price information. For an electronic copy visit the MSA web site at <http://www.minsocam.org>, go to the *American Mineralogist* Contents, find the table of contents for the specific volume/issue wanted, and then click on the deposit link there.

TABLE 9. Assignments of the infrared frequencies (cm^{-1}) for the $\text{Na}_2(\text{Mn}_{1-x}\text{M}_x^{2+})\text{Fe}^{2+}\text{Fe}^{3+}(\text{PO}_4)_3$ ($M^{2+} = \text{Cd, Mg}$) alluaudite-type compounds

$x = 0.00$	0.25	0.50	0.75	1.00	Difference	Assignments
$\text{Na}_2(\text{Mn}_{1-x}\text{Cd}_x)\text{Fe}^{2+}\text{Fe}^{3+}(\text{PO}_4)_3$						
1384	1384	1384	1384	1384	0	
1097	1090	1089	1089	1089	-8	
1044	1034	1032	1032	1032	-12	$\nu_3\text{ PO}_4$
993	997	996	997	1001	8	
941	941	942	945	944	3	
924						
634	634	628	628		-6	$\text{Fe}^{3+}\text{-O}$
596	600	600	602	601	5	$M^{2+}\text{-O on M2}$
581	582	582	583	585	4	
				569		$\nu_4\text{ PO}_4$
545	546	546	546	546	1	
520	518	514	515	514	-6	
				471		
465	463	463	463		-2	$\text{Fe}^{3+}\text{-O}$ or PO_4 bending?
422	420	417	413	409	-13	$M^{2+}\text{-O on M1}$
$\text{Na}_2(\text{Mn}_{1-x}\text{Mg}_x)\text{Fe}^{2+}\text{Fe}^{3+}(\text{PO}_4)_3$						
1384	1384	1384	1384	1384	0	
		1156	1148	1150	-6	
1097						
	1088	1087	1090	1090	2	
1044	1038				-6	$\nu_3\text{ PO}_4$
993	997	1000	1003	997	4	
941	936	927			-14	
924						
		911	912	900	-11	$\nu_1\text{ PO}_4$
634	636	638	640	642	8	$\text{Fe}^{3+}\text{-O}$
596	602	604	608	610	14	$M^{2+}\text{-O on M2}$
581	577	573	575	572	-9	
545	547	546	547	548	3	$\nu_4\text{ PO}_4$
520	514	516	516	516	-4	
465	462	462	464		-1	$\text{Fe}^{3+}\text{-O}$ or PO_4 bending?
422	429	430	437	443	21	$M^{2+}\text{-O on M1}$

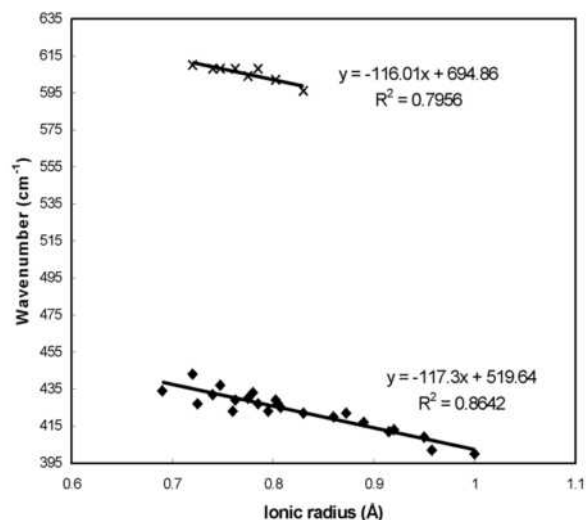


FIGURE 9. Correlation between wavenumber of the infrared absorption bands located around 405–445 and 595–610 cm^{-1} , and the average ionic radius of the cations occurring on the M1 and M2 sites, for the $\text{Na}_2(\text{Mn}_{1-x}\text{M}^{2+})\text{Fe}^{2+}\text{Fe}^{3+}(\text{PO}_4)_3$ ($\text{M}^{2+} = \text{Ni}, \text{Mg}, \text{Zn}, \text{Cd}, \text{Ca}$) solid solutions.

In the $\text{Na}_2(\text{Mn}_{1-x}\text{Mg}_x)\text{Fe}^{2+}\text{Fe}^{3+}(\text{PO}_4)_3$ solid solution, another band, located at 596 cm^{-1} when $x = 0$, also shifts significantly toward high wavenumbers when x increases. This band can be assigned to the vibrations of the M^{2+} cations localized on the M2 site, since the Mn-Mg substitution also takes place on M2 in the $\text{Na}_2(\text{Mn}_{1-x}\text{Mg}_x)\text{Fe}^{2+}\text{Fe}^{3+}(\text{PO}_4)_3$ solid solution. This assignment is further confirmed by the satisfactory correlation between the average ionic radii of M2 cations and the wavenumber of this absorption band (Fig. 9).

Qualitatively, it is noteworthy that the infrared absorption bands in the $\text{Na}_2(\text{Mn}_{1-x}\text{Mg}_x)\text{Fe}^{2+}\text{Fe}^{3+}(\text{PO}_4)_3$ solid solution are much broader than those of $\text{Na}_2(\text{Mn}_{1-x}\text{Cd}_x)\text{Fe}^{2+}\text{Fe}^{3+}(\text{PO}_4)_3$ (Figs. 6 and 7). This behavior certainly results from the disordered distribution of Fe and Mg on the M1 and M2 sites in $\text{Na}_2(\text{Mn}_{1-x}\text{Mg}_x)\text{Fe}^{2+}\text{Fe}^{3+}(\text{PO}_4)_3$, whereas M2 is occupied by Fe only in $\text{Na}_2(\text{Mn}_{1-x}\text{Cd}_x)\text{Fe}^{2+}\text{Fe}^{3+}(\text{PO}_4)_3$ (Tables 5 and 6).

ACKNOWLEDGMENTS

The authors are indebted to A.-M. Franolet, P. Schmid-Beurmann, P. Keller, and M. Kunz for their constructive comments on the earlier versions of this manuscript. The “Fonds National de la Recherche Scientifique” (Belgium) is acknowledged for a position of “Chercheur Qualifié” and for grants 1.5.113.05.F, 1.5.098.06.F, and 1.5.112.02.

REFERENCES CITED

Antenucci, D. (1992) Synthèse et cristallographie de composés à structure alluaudite. Incidences dans les processus d'altération des phosphates Fe-Mn des pegmatites granitiques, 259 p. Ph.D. thesis, University of Liège, Belgium.

Antenucci, D., Miehé, G., Tarte, P., Schmahl, W.W., and Franolet, A.-M. (1993) Combined X-ray Rietveld, infrared and Raman study of a new synthetic variety of alluaudite, $\text{NaCdIn}_2(\text{PO}_4)_3$. *European Journal of Mineralogy*, 5, 207–213.

Antenucci, D., Franolet, A.-M., Miehé, G., and Tarte, P. (1995) Synthèse et cristallographie de $\text{NaCaCdMg}_2(\text{PO}_4)_3$, phosphate nouveau à structure alluaudite sans cation trivalent. *European Journal of Mineralogy*, 7, 175–181.

Auernhammer, M., Effenberger, H., Hentschel, G., Reinecke, T., and Tillmanns, E. (1993) Nickenichite, a new arsenate from the Eifel, Germany. *Mineralogy and Petrology*, 48, 153–166.

Brown, I.D. and Altermatt, D. (1985) Bond-valence parameters obtained from a systematic analysis of the inorganic crystal structure database. *Acta Crystallographica*, B41, 244–247.

Brunet, F., Chopin, C., and Seifert, F. (1998) Phase relations in the $\text{MgO-P}_2\text{O}_5\text{-H}_2\text{O}$ system and the stability of phosphoellenbergerite: Petrological implications. *Contributions to Mineralogy and Petrology*, 131, 54–70.

Burnham, C.W. (1991) LCLSQ version 8.4, least-squares refinement of crystallographic lattice parameters, 24 p. Department of Earth and Planetary Sciences, Harvard University.

Černý, P. and Ercit, T.S. (2005) The classification of granitic pegmatites revisited. *Canadian Mineralogist*, 43, 2005–2026.

Farmer, V.C. (1974) *The Infrared Spectra of Minerals*, 539 p. Mineralogical Society Monographs, London.

Franolet, A.-M., Keller, P., and Fontan, F. (1986) The phosphate mineral associations of the Tsaobismund pegmatite, Namibia. *Contributions to Mineralogy and Petrology*, 92, 502–517.

Franolet, A.-M., Fontan, F., Keller, P., and Antenucci, D. (1998) La série johnsomervilleite-fillowite dans les associations de phosphates de pegmatites granitiques de l'Afrique centrale. *Canadian Mineralogist*, 36, 355–366.

Guesmi, A. and Driss, A. (2002) $\text{AgCo}_3\text{PO}_4(\text{HPO}_4)_2$. *Acta Crystallographica*, C58, i16–i17.

Hatert, F. (2002) Cristallographie et synthèse hydrothermale d'alluaudites dans le système Na-Mn-Fe-P-O: Contribution au problème de la genèse de ces phosphates dans les pegmatites granitiques, 247 p. Ph.D. thesis, University of Liège, Belgium.

——— (2004) The crystal chemistry of lithium in the alluaudite structure: a study of the $(\text{Na}_{1-x}\text{Li}_x)_5\text{Mn}_3\text{Fe}_{15}^{2+}(\text{PO}_4)_3$ solid solution ($x = 0$ to 1). *Mineralogy and Petrology*, 81, 205–217.

——— (2008) The crystal chemistry of the divalent cation in alluaudite-type phosphates: A structural and infrared spectral study of the $\text{Na}_{15}(\text{Mn}_{1-x}\text{M}^{2+})_3\text{Fe}_{15}(\text{PO}_4)_3$ solid solutions ($x = 0$ to 1, $\text{M}^{2+} = \text{Cd}^{2+}, \text{Zn}^{2+}$). *Journal of Solid State Chemistry*, 181, 1258–1272.

Hatert, F., Keller, P., Lissner, F., Antenucci, D., and Franolet, A.-M. (2000) First experimental evidence of alluaudite-like phosphates with high Li-content: the $(\text{Na}_{1-x}\text{Li}_x)\text{MnFe}_2(\text{PO}_4)_3$ series ($x = 0$ to 1). *European Journal of Mineralogy*, 12, 847–857.

Hatert, F., Antenucci, D., Franolet, A.-M., and Liègeois-Duyckaerts, M. (2002) The crystal chemistry of lithium in the alluaudite structure: A study of the $(\text{Na}_{1-x}\text{Li}_x)\text{CdIn}_2(\text{PO}_4)_3$ solid solution ($x = 0$ to 1). *Journal of Solid State Chemistry*, 163, 194–201.

Hatert, F., Hermann, R.P., Long, G.J., Franolet, A.-M., and Grandjean, F. (2003) An X-ray Rietveld, infrared, and Mössbauer spectral study of the $\text{NaMn}(\text{Fe}_{1-x}\text{In}_x)_2(\text{PO}_4)_3$ alluaudite-type solid solution. *American Mineralogist*, 88, 211–222.

Hatert, F., Long, G.J., Hautot, D., Franolet, A.-M., Delwiche, J., Hubin-Franskin, M.J., and Grandjean, F. (2004) A structural, magnetic, and Mössbauer spectral study of several Na-Mn-Fe-bearing alluaudites. *Physics and Chemistry of Minerals*, 31, 487–506.

Hatert, F., Rebbouh, L., Hermann, R.P., Franolet, A.-M., Long, G.J., and Grandjean, F. (2005) Crystal chemistry of the hydrothermally synthesized $\text{Na}_2(\text{Mn}_{1-x}\text{Fe}_x)_2\text{Fe}^{3+}(\text{PO}_4)_3$ alluaudite-type solid solution. *American Mineralogist*, 90, 653–662.

Hatert, F., Franolet, A.-M., and Maresch, W.V. (2006) The stability of primary alluaudites in granitic pegmatites: An experimental investigation of the $\text{Na}_2(\text{Mn}_{1-x}\text{Fe}_x)_2\text{Fe}^{3+}(\text{PO}_4)_3$ solid solution. *Contributions to Mineralogy and Petrology*, 152, 399–419.

Hermann, R.P., Hatert, F., Franolet, A.-M., Long, G.J., and Grandjean, F. (2002) Mössbauer spectral evidence for next-nearest neighbor interactions within the alluaudite structure of $\text{Na}_{1-x}\text{Li}_x\text{MnFe}_2(\text{PO}_4)_3$. *Solid State Sciences*, 4, 507–513.

Hidouri, M., Lajmi, B., Wattiaux, A., Fournés, L., Darriet, J., and Amara, M.B. (2004) Characterization by X-ray diffraction, magnetic susceptibility and Mössbauer spectroscopy of a new alluaudite-like phosphate: $\text{Na}_4\text{CaFe}_4(\text{PO}_4)_6$. *Journal of Solid State Chemistry*, 177, 55–60.

Kacimi, M., Ziyad, M., and Hatert, F. (2005) Structural features of $\text{AgCaCdMg}_2(\text{PO}_4)_3$ and $\text{AgCd}_2\text{Mg}_2(\text{PO}_4)_3$, two new compounds with the alluaudite-type structure, and their catalytic activity in butan-2-ol conversion. *Materials Research Bulletin*, 40, 682–693.

Keller, P. and Hess, H. (1988) Die Kristallstrukturen von O'Danielit, $\text{Na}(\text{Zn}, \text{Mg})_2\text{H}_2(\text{AsO}_4)_3$, und Johillerit, $\text{Na}(\text{Mg}, \text{Zn})\text{Cu}(\text{AsO}_4)_3$. *Neues Jahrbuch für Mineralogie, Monatshefte*, 395–404.

Keller, P., Riffel, H., Zettler, F., and Hess, H. (1981) $\text{AgCo}_3\text{H}_2(\text{AsO}_4)_3$ und $\text{AgZn}_3\text{H}_2(\text{AsO}_4)_3$. Darstellung und Kristallstruktur. Ein Weiterer neuer Arsenat-Strukturtyp. *Zeitschrift für anorganische und allgemeine Chemie*, 474, 123–134.

Korzenski, M.B., Schimek, G.L., Kolis, J.W., and Long, G.J. (1998) Hydrothermal synthesis, structure, and characterization of a mixed-valent iron (II/III) phosphate, $\text{NaFe}_{3.67}(\text{PO}_4)_3$: a new variation of the alluaudite structure type. *Journal of Solid State Chemistry*, 139, 152–160.

Leroux, F., Mar, A., Payen, C., Guyomard, D., Verbaere, A., and Piffard, Y. (1995a) Synthesis and structure of $\text{NaMn}_3(\text{PO}_3)(\text{HPO}_4)_2$, an oxidized variant of the alluaudite structure type. *Journal of Solid State Chemistry*, 115, 240–246.

- Leroux, F., Mar, A., Guyomard, D., and Piffard, Y. (1995b) Cation substitution in the alluaudite structure type: Synthesis and structure of $\text{AgMn}_3(\text{PO}_4)(\text{HPO}_4)_2$. *Journal of Solid State Chemistry*, 117, 206–212.
- Lii, K.H. and Shih, P.F. (1994) Hydrothermal synthesis and crystal structures of $\text{NaCo}_3(\text{PO}_4)(\text{HPO}_4)_2$ and $\text{NaCo}_3(\text{AsO}_4)(\text{HAsO}_4)_2$: Synthetic modifications of the mineral alluaudite. *Inorganic Chemistry*, 33, 3028–3031.
- London, D., Wolf, M.B., Morgan, G.B., and Gallego Garrido, M. (1999) Experimental silicate-phosphate equilibria in peraluminous granitic magmas, with a case study of the Albuquerque batholith at Tres Arroyos, Badajoz, Spain. *Journal of Petrology*, 40, 215–240.
- London, D., Morgan, G.B., and Wolf, M.B. (2001) Amblygonite-montebasite solid solutions as monitors of fluorine in evolved granitic and pegmatitic melts. *American Mineralogist*, 86, 225–233.
- Moore, P.B. (1971) Crystal chemistry of the alluaudite structure type: Contribution to the paragenesis of pegmatite phosphate giant crystals. *American Mineralogist*, 56, 1955–1975.
- Moore, P.B. and Ito, J. (1979) Alluaudites, wyllieites, arrojadites: Crystal chemistry and nomenclature. *Mineralogical Magazine*, 43, 227–235.
- Redhammer, G.J., Tippelt, G., Bernroider, M., Lottermoser, W., Amthauer, G., and Roth, G. (2005) Hagendorfite $(\text{Na,Ca})\text{MnFe}_2(\text{PO}_4)_3$ from type locality Hagendorf (Bavaria, Germany): Crystal structure determination and ^{57}Fe Mössbauer spectroscopy. *European Journal of Mineralogy*, 17, 915–932.
- Richardson, T.J. (2003) Phosphate-stabilized lithium intercalation compounds. *Journal of Power Sources (Selected papers presented at the 11th International Meeting on Lithium Batteries)*, 119–121, 262–265.
- Riffel, H., Keller, P., and Hess, H. (1985) Die Kristallstruktur von $\text{AgCu}_3\text{Cu}(\text{AsO}_4)_3$ und ihre strukturellen Beziehungen zu $\text{AgCo}_3\text{H}_2(\text{AsO}_4)_3$ bzw. $\text{AgZn}_3\text{H}_2(\text{AsO}_4)_3$. *Zeitschrift für anorganische und allgemeine Chemie*, 530, 60–68.
- Roda Robles, E., Fontan, F., Pesquera Pérez, A., and Keller, P. (1998) The Fe-Mn phosphate associations from the Pinilla de Fermoselle pegmatite, Zamora, Spain: Occurrence of kryzhanovskite and natrodufrénite. *European Journal of Mineralogy*, 10, 155–167.
- Shannon, R.D. (1976) Revised effective ionic radii and systematic studies of interatomic distances in halides and chalcogenides. *Acta Crystallographica*, A32, 751–767.
- Solodovnikov, S.F., Klevtsov, P.V., Solodovnikova, Z.A., Glinskaya, L.A., and Klevtsova, R.F. (1998) Binary molybdates $\text{K}_4\text{M}^{2+}(\text{MoO}_4)_3$ ($\text{M}^{2+} = \text{Mg, Mn, Co}$) and crystal structure of $\text{K}_4\text{Mn}(\text{MoO}_4)_3$. *Journal of Structural Chemistry*, 39, 230–237.
- Tsyrenova, G.D., Solodovnikov, S.F., Zolotova, E.S., Tsybikova, B.A., and Bazarova, Z.G. (2000) Phase formation in the $\text{K}_2\text{O}(\text{K}_2\text{CO}_3)\text{-CdO-MoO}_3$ system. *Russian Journal of Inorganic Chemistry*, 45, 103–108.
- Tuttle, O.F. (1949) Two pressure vessels for silicate-water studies. *Geological Society of America Bulletin*, 60, 1727–1729.
- Young, R.A., Larson, A.C., and Paiva-Santos, C.O. (1998) User's guide to program DBWS-9807 for Rietveld analysis of X-ray and neutron powder diffraction patterns, 56 p. Georgia Institute of Technology, Atlanta.
- Zid, M.F., Driss, A., and Jouini, T. (2005) $(\text{Na}_{0.38}\text{Ca}_{0.31})\text{MgFe}_2\text{P}_3\text{O}_{12}$. *Acta Crystallographica*, E61, i46–i48.

MANUSCRIPT RECEIVED AUGUST 6, 2009

MANUSCRIPT ACCEPTED JANUARY 14, 2010

MANUSCRIPT HANDLED BY MATTHIAS GOTTSCHALK